Concerted Hydrogen Exchange Tunneling in Formic Acid Dimer†

David Luckhaus‡

Department of Chemistry, University of British Columbia, 2036 Main Mall, Vancouver, B.C., Canada V6T 1Z1

Received: August 13, 2005; In Final Form: November 3, 2005

The effect of conformational relaxation on the quantum dynamics of the hydrogen exchange tunneling is studied in the D_{2h} subspace of formic acid dimer. The fully coupled quantum dynamics in up to six dimensions are derived for potential energy hypersurfaces interpolated directly from hybrid density functional calculations with and without geometry relaxation. For a calculated electronic barrier height of 35.0 kJ/mol the vibrational ground state shows a tunneling splitting of 0.0013 cm^{-1}. The results support the vibrational assignment of Madeja and Havenith [*J. Chem. Phys*. **2002**, *117*, 7162−7168]. Fully coupled ro-vibrational calculations demonstrate the compatibility of experimentally observed inertia defects with in-plane hydrogen exchange tunneling dynamics in formic acid dimer.

1. Introduction

Small hydrogen-bonded systems are ideal objects for studying fundamental aspects of chemical reaction dynamics, in particular those regarding the role of intramolecular vibrational energy redistribution (IVR). This comprises phenomena such as the hierarchy of time scales for intramolecular energy redistribution (IVR), vibrational adiabaticity, and mode specificity of reaction dynamics.

One specific feature that has attracted much attention is the hydrogen or proton transfer tunneling. Small molecular systems are quoted as models for such processes in larger biological systems. Hydrogen exchange tunneling systems offer the particular advantage of direct spectroscopic access to the reactive (i.e., hydrogen exchange tunneling) process. Its interplay with IVR and with the heavy frame conformational dynamics can be observed directly by ro-vibrational spectroscopy through the vibrational dependence of tunneling splittings. For the interpretation of the results a detailed model of the underlying quantum dynamics is evidently essential. This extends to the rather practical question of which modes are essential in the sense that they would have to be included explicitly in the active system part of any realistic system/bath (or quantum/classical) type model for larger biological systems.

As the simplest prototype system showing concerted intermolecular hydrogen exchange, formic acid dimer (FAD) has attracted considerable interest over the years. Thus, it had been speculated about the possible contribution of the exchange tunneling to the enormous broadening of the infrared absorption spectrum in the range of the OH-stretching fundamental, whose excitation energy coincides roughly with the estimated barrier for this process.[1] This spectral feature is characteristic for carboxylic acid dimers in general, but has recently been traced back to essentially intramolecular anharmonic resonances within the vibrational subspace of the monomeric carboxyl groups.[2−4] The first experimental values for the tunneling splitting in the electronic ground state of FAD—in fact of any carboxylic acid dimer—were recently derived by Madeja and Havenith from high-resolution ro-vibrational spectroscopy.[5] The results appear to confirm theoretical predictions by Shida and Almlöf,[6] although the assignment of the two experimental values to the vibrational states involved, viz. the ground state and the C−O stretching fundamental, remains ambiguous.[5,7,8] There have been many theoretical attempts to predict the ground state tunneling splitting invoking approximations of widely varying quality. The conceptually more convincing approaches include the pure quantum-mechanical reaction-surface model of Shida and Almlöf[6] as well as the semiclassical approaches of Tautermann et al.[7] and of Smedarchina et al.[8] Given the complexity of the system (24 vibrational degrees of freedom), the quantum mechanical treatment of the dynamics has to rely on some form of reduced dimensionality approximation. So far, only the semiclassical models can afford to avoid this approximation (but obviously have to make others instead).[7,8] The quantitative reliability, however, of semiclassical models for hydrogen tunneling processes has become the subject of some discussion after the direct comparison with corresponding fully quantum mechanical calculations has recently become possible for a truly multidimensional system—in this case for malonaldehyde.[9] Moreover, different semiclassical models apparently come to different conclusions for the assignment of the experimental values for the tunneling splitting in FAD. A quantum mechanical treatment is clearly desirable, but is has to rely on reduced dimensionality approaches as long as numerical calculations in full dimensionality remain out of reach. Even once they become feasible it is still important to search for approximate separability in the system since it implies approximate symmetries and constants of the motion, i.e., the "nontrivial" part of the dynamics.

The subject of this contribution is a systematic study of reduced dimensionality models for the proton exchange tunneling in FAD, to identify the most relevant degrees of freedom, in particular the role of the geometry relaxation of the molecular frame in the course of the tunneling process. As the rotational analysis of the experimental spectra has led to some speculation about the involvement of nonplanar structures, it will be shown that the significant inertial defects derived from experimental observations are perfectly consistent even with strictly in-plane tunneling dynamics.

† Part of the special issue "Jürgen Troe Festschrift".

‡ Telephone: +1604 827 5650. E-mail: dluckhaus@chem.ubc.ca.

10.1021/jp054558a CCC: $33.50
Published on Web 12/09/2005

TABLE 1: Calculated Geometries (EQ = Equilibrium, TS = Transition State) and Rotational Constants

	B3LYP/6-31+G*		B3LYP/6-31++G**		MP2/6-311++G** [a]		expt[b,c]
	EQ	TS	EQ	TS	EQ	TS	EQ
x_H/Å	0.424	0.0	0.421	0.0	0.449	0.0	0.380
z_H/Å	1.189	1.118	1.189	1.115	1.178	1.101	1.151
Δr/Å	0.094	0.0	0.096	0.0	0.098	0.0	0.104
r/Å	1.271	1.267	1.266	1.261	1.270	1.264	1.269
β_R/deg	4.531	0.0	4.753	0.0	5.33	0.0	4.53
β/deg	126.25	126.60	126.22	126.60	126.15	126.92	126.20
R/Å	3.855	3.569	3.826	3.552	3.843	3.532	3.827
r_{CH}/Å	1.097	1.096	1.096	1.095	1.095	1.094	1.089
α/deg	0.68	0.0	0.50	0.0	0.20	0.0	0.67
A^c/cm^{-1}	0.200 28		0.202 19		0.201 57		0.20154 (0.20205)[d]
B^c/cm^{-1}	0.068 60		0.069 62		0.068 81		0.06976 (0.07059)[d]
C^c/cm^{-1}	0.051 10		0.051 79		0.051 30		0.05182 (0.05237)[d]

[a] Core electrons frozen. MP2/TZ2P calculations (polarized valence triple-ζ basis without diffuse functions[27]) yielded the following equilibrium structure: $x_H = 0.508$ Å, $z_H = 1.212$ Å, $\Delta r = 0.095$ Å, $\beta_R = 4.05°$, $R = 3.80$ Å, $r_{CH} = 1.089$ Å, $\alpha = 1.25°$. [b] Electron diffraction data from ref 28. Rotational constants calculated from this geometry for $(DCOOH)_2$. [c] Rotational constants calculated from the equilibrium geometry for $(DCOOH)_2$. [d] Experimental rotational constants determined for $(DCOOH)_2$ from ro-vibrational spectroscopy[5] are given in parentheses. Rotational constants for $(HCOOH)_2$ have recently been determined from time-resolved spectroscopy:[29] 0.020227, 0.07679, 0.05554 cm^{-1}.

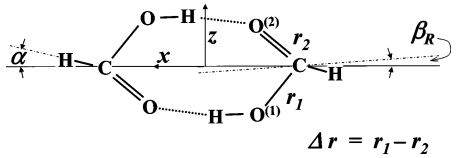

Figure 1. Definition of coordinates for C_{2h} FAD: Cartesian axes (x, z) (origin at the center of mass, x along CC), (x_H, z_H) = Cartesian coordinates of the bonding H atoms, (r,Δr) = symmetric and antisymmetric OCO stretch, β = OCO bend, $\beta_R = \angle CCO^{(1)} - \angle CCO^{(2)}$ = intermolecular bend, R = C−C distance, r_{CH} = CH bond length, $\alpha = \angle O^{(2)}CH + \angle CCO^{(2)} - 180°$ = CCH bend.

2. Theoretical Methods

Given the strength of the double hydrogen bond and the overall valence structure of FAD, the planarity is expected to be retained during the tunneling process. This view is supported by all ab initio quantum chemical calculations so far performed for the tunneling path, irrespective of the level of theory.[10,11] In line with these findings, the present investigation is limited to planar geometries retaining local C_{2h} point group symmetry. The saddle point has D_{2h} point group symmetry which is isomorphic to the molecular symmetry group G_8 of FAD undergoing concerted intermolecular hydrogen exchange.

2.1. Coordinates and Potential Energy Functions. There is a total of nine coordinates that are totally symmetric under C_{2h} point group operations in FAD (i.e., that retain the local point group symmetry). Figure 1 illustrates the choice of coordinates for the present investigation: a combination of Cartesian coordinates (x_H, z_H) for the exchanging hydrogen atoms and valence coordinates (bond lengths, bond angles) for the HCO_2 moieties, which remain intact during the process. The molecule is chosen to lie in the (x, z)-plane with the x-axis defined by the line connecting the C atoms. The valence coordinates for the HCO_2-moieties are the two CO-bond lengths r_1 and r_2, the OCO-bond angle β, the CH-bond length r_{CH}, and the angle α between the CH-bond and the x-axis. The symmetric combination of the CO-bond lengths stays virtually constant along the reaction path so that only the antisymmetric combination $\Delta r = r_1 - r_2$ is considered here. The intermolecular geometry parameters are the C−C-distance R and the intermolecular bending angle β_R between the bisector of the OCO bond angle and the x-axis.

The particular definition of the CH bend as the CCH bond angle does not follow the corresponding normal coordinate particularly well, but it has the advantage of remaining virtually constant along the intrinsic reaction coordinate. The price to pay is some minor mixing between the intermolecular bend and the CH bend modes. Symmetry adaptation is obtained by enforcing identical values for symmetry equivalent pairs of coordinates.

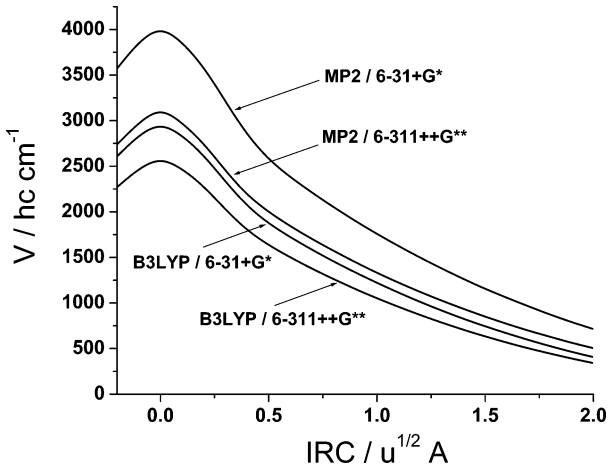

Figure 2. Potential energy profile along the intrinsic reaction coordinate of the concerted hydrogen exchange in formic acid dimer calculated at different levels of theory.

To minimize the influence of inaccuracies in the representation of the underlying 24 dimensional potential function the successively averaged spline interpolation (SASI) scheme was employed. The procedure has been described in more detail in ref 12. The various reduced dimensionality model potentials are interpolated directly from a table of quantum chemical single point calculations. The large number of such calculations required for an accurate representation of the potential function ($\sim 10^6$ in 6D) necessitates judicious optimization of the quantum chemical part of the calculations. Figure 2 shows the potential energy profile along the intrinsic reaction coordinate (defined by the mass-weighted steepest descent from the saddle point) derived on various levels of theory. The change of geometry in terms of the coordinates defined in Figure 1 is very similar in all cases as born out by the comparison of equilibrium and saddle point geometries in Table 1. The best theoretical estimate of the (purely electronic) barrier height is 2760 cm^{-1} or 33.0 kJ/mol (geometry optimized at the MP2 level followed by a single point energy calculation using CCSD(T), both with the aug-cc-pVTZ basis set).[11] In terms of both barrier height and barrier width the B3LYP hybrid density functional with the

TABLE 2: Calculated Harmonic Wavenumbers $\tilde{\omega}$ (EQ = Equilibrium, TS = Transition State) and Barrier Heights ΔE

	$\tilde{\omega}_g/\tilde{\omega}_u$						
	B3LYP/6-31G*		B3LYP/6-311++G**		MP2/6-311++G** [a]		expt[b]
parameters[c]	EQ	TS	EQ	TS	EQ	TS	(EQ)
β_R[d]	170/269	231/551	168/260	230/574	162/243	225/592	190/248
β_R[d]	210/...	492/...	200/...	508/...	189/...	524/...	137/...
β_{OCO}	678/704	737/791	684/711	749/794	684/703	752/796	677/699
β_{C-O}	1254/1255	1400/1400	1248/1251	1397/1400	1253/1258	1411/1428	1214/1218
β_{CH}	1405/1397	1405/1406	1394/1391	1401/1401	1415/1406	1427/1427	1375/1362
β_{OH}	1461/1441	1640/1538	1459/1438	1657/1558	1481/1461	1704/1601	1415/...
$\nu_{C=O}$	1723/1786	1751/1738	1706/1773	1739/1727	1732/1789	1773/1761	1670/1754
ν_{CH}	3118/3113	3130/3128	3074/3069	3083/3082	3145/3141	3155/3154	2949/2957
ν_{OH}	3156/3247	1319i/1198	3165/3261	1253i/1257	3334/3417	1351i/1288	.../3110
τ_R	.../78	.../90	.../76	.../86	.../56	.../58	.../68
δ_R	257/180	308/233	249/175	302/233	216/160	297/228	230/163
δ_{OH}	956/982	1070/1063	942/973	1070/1066	896/926	1078/1068	.../917
δ_{CH}	1069/1090	1281/1335	1070/1091	1302/1361	1074/1101	1294/1383	1050/1060
ΔE		2930		2558		3091	

[a] Core electrons frozen. [b] Experimental data from refs 30, 31, and 32 as cited in ref 4 (see also ref 13 and references therein). [c] Wavenumbers are given in cm^{-1} for u/g pairs. Experimental values are fundamental transition wavenumbers. Vibrational assignment: ν = stretch, β/δ = in/out−of−plane bend, t = torsion, index R for intermolecular modes. ν_{C-O} correlates with the transition state's symmetric and $\nu_{C=O}$ with its antisymmetric OCO-stretching mode. In plane vibrations transform as A_g or B_u, out−of−plane vibrations as B_g or A_u. [d] The assignment of calculated gerade in−plane intermolecular bend (β_R) and stretch (ν_R) normal modes are switched in ref 4.

6-31+G* basis set evidently compares very favorably with much higher level calculations. This is also evident from the comparison of harmonic wavenumbers and barrier heights in Table 2. At 10−20 s per point on a standard personal computer, it recommends itself as a suitable compromise between theoretical rigor and computational effort. It is interesting to note that the assignment of the gerade intermolecular in-plane bend β_R and stretch ν_R is interchanged compared with that given in ref 4. The assignment is obvious from the inspection of the displacement vectors. It is also confirmed by the vibrational calculations performed in the present investigation: The 4D flexible model including x, Δr, β_R, and R yields anharmonic wavenumbers of 212 cm^{-1} for ν_R and 167 cm^{-1} for β_R. Thus, the intermolecular bend lies below the intermolecular stretch. Judging from the harmonic wavenumbers given in Table 2 this ordering should be retained at higher levels of ab initio theory. This result sheds some doubt on the currently accepted assignment of experimental values.[13]

Relaxed potential surfaces—minimum energy, paths, surfaces, volumes, etc.—were calculated for fixed values of the active coordinates by minimizing the electronic energy with respect to all remaining degrees of freedom while conserving C_{2v} point group symmetry.

In all cases the grid points for which electronic calculations were performed were chosen by starting from a set of reference points (i.e., those already calculated) and selecting the missing next nearest neighbors with the lowest energy estimates. Those estimates were taken themselves as the average of next nearest neighbors within the set of reference points. The procedure always started from the equilibrium geometry. Table 3 lists the grid parameters for each model. Application of the SASI scheme for further refinement of the grids finally yielded the grid representation of the various model potentials used further on in the vibrational calculations. The overall convergence of the grid representation of the model potential was checked with respect to both extending the "ab initio" data set and increasing the grid resolution of the SASI scheme.

2.2. Ro-Vibrational Calculations. With the help of pseudo atoms the vibrational coordinates were defined formally in terms of local polar coordinates ("*Z*-matrix coordinates") so that the geometry dependent terms in the kinetic energy operator could be calculated automatically using the generalized *Z*-matrix

TABLE 3: DVR Grids and Basis Set Truncation Parameters Used for Different Multidimensional Models of the Symmetric Proton Exchange Tunneling in FAD

q	q_{min}	q_{max}	N_q[a]	Δq
x/Å	−1.30	1.30	53	0.050
z/Å	0.70	1.90	13	0.100
Δr/Å	−0.30	0.30	25	0.025
r/Å	1.169	1.469	13	0.025
β/deg	110.254	142.254	9	2.000
β_R/deg	−30.0	30.0	61	1.000
R/Å	3.00	4.60	33	0.025

	coordinates	V_{max}/cm^{-1} [b]	N[c]	E_{max}/cm^{-1} [d]	N_{bas}[e]
2D	(r_{OH}, R)	300 000	2805	40 000	2214
	(x, r)	31 500	2475	38 000	1048
3D	(x, β_R, R)	30 000	21 629	25 000	2219
	(x, z, R)	30 000	10 638	21 400	3069
	(x, Δr, R)	30 000	6592	21 400	1523
4D	(x, Δr, β_R, R)	30 000	243 658	12 100	6449
5D	(x, z, Δr, β_R, R)	20 000	384 069	11 000	8951
6D	(x, z, Δr, β, β_R, R)	15 000	1778323	11 000	5065

[a] Number of grid points in 1D. [b] Potential energy cut-off value. [c] Total number of DVR grid points included in the calculation (=primitive DVR basis size). [d] Energy cut-off for basis functions in the last truncation step. [e] Number of basis functions in the final diagonalization step.

discrete variable representation (DVR) described in ref 14. The implementation of the Chebychev−DVR follows the original scheme proposed by refs 15 and 16. The generalized coordinate formalism is an extension of the approach introduced by Meyer and Günthard.[17,18] Within this formalism the full ro-vibrational Hamiltonian for a molecule with N atoms is given by the following expression:

$$\hat{H} = \frac{1}{2}(\hat{\mathbf{J}}^t, \hat{\mathbf{p}}^t)\begin{pmatrix}\mu & \mathbf{Z}^t \\ \mathbf{Z} & \mathbf{G}\end{pmatrix}\begin{pmatrix}\hat{\mathbf{J}} \\ \hat{\mathbf{p}}\end{pmatrix} + u(\mathbf{q}) + V(\mathbf{q}) \qquad (1)$$

where $\boldsymbol{A}^t$ denotes the transpose of a matrix or vector $\boldsymbol{A}$. $\hat{J}_\alpha$ are molecule-fixed Cartesian components of the angular momentum operator, q_k are generalized internal (=vibrational) coordinates, and $\hat{p}_k = -i\hbar\partial/\partial q_k$ are the conjugate vibrational momentum operators. $\hbar$ is Planck's constant devided by 2π. V is the potential energy and u is the pseudo-potential, which results from the curvature of the rotational and vibrational coordinates,

but only depends on the latter.[18] As discussed in ref 14 it has numerical advantages to rewrite the purely vibrational Hamiltonian in the following way:

$$\hat{H}_{vib} = \frac{1}{4}\left(\sum_{k,l}\{\hat{p}_k\hat{p}_l, G_{kl}\} + \hbar^2\frac{\partial^2 G_{kl}}{\partial q_k \partial q_l}\right) + u' + V \qquad (2)$$

where $\{A, B\} = AB + BA$ is the anti-commutator of A and B, and u' is a slightly modified pseudo-potential (see also ref 12)

$$u(q_1, q_2, \ldots) = \frac{\hbar^2}{8}\sum_{k,l}\frac{\partial\{G_{kl}\cdot d_l\}}{\partial q_k} + d_k\cdot\frac{G_{kl}}{4}\cdot d_l \qquad (3)$$

$$d_k = \frac{\partial}{\partial q_k}\ln\begin{vmatrix}\mathbf{I} & \mathbf{C}\\ \mathbf{C}^t & \mathbf{g}\end{vmatrix} \qquad (4)$$

where $|\mathbf{A}|$ is the determinant of $\mathbf{A}$. The tensor of inertia $\boldsymbol{I}$, the Coriolis coupling $\boldsymbol{C}$ and the vibrational tensor $\boldsymbol{g}$ together form the covariant metric tensor. Their elements are given in terms of the rotating molecule-fixed Cartesian axes $\vec{e}_\alpha$, the atomic coordinate vectors $\vec{x}_i$ with respect to this basis, and the atomic masses m_i:

$$I_{\alpha\beta} = \sum_{i=1}^{N} m_i(\vec{e}_\alpha \otimes \vec{x}_i)^t(\vec{e}_\beta \otimes \vec{x}_i) \qquad (5)$$

$$C_{\alpha k} = \sum_{i=1}^{N} m_i(\vec{e}_\alpha \otimes \vec{x}_i)^t\frac{\partial \vec{x}_i}{\partial q_k} \qquad (6)$$

$$g_{kl} = \sum_{i=1}^{N} m_i\frac{\partial \vec{x}_i^t}{\partial q_k}\cdot\frac{\partial \vec{x}_i}{\partial q_l} \qquad (7)$$

As proposed by Meyer and Günthard[17] the contravariant metric tensor elements $\mu_{\alpha\beta}$, $Z_{k\alpha}$, and G_{kl} are obtained by pointwise inversion of the corresponding covariant tensor:

$$\begin{pmatrix}\mu & \mathbf{Z}^t\\ \mathbf{Z} & \end{pmatrix} = \begin{pmatrix}\mathbf{I} & \mathbf{C}\\ \mathbf{C}^t & g\end{pmatrix}^{-1} \qquad (8)$$

μ corresponds to the effective inverse tensor of inertia. The derivatives $\partial\vec{x}_i/\partial q_k$ can now be calculated analytically for the geometry defined in terms of local polar coordinates as a function of the active coordinates q_k.[14,19,12]

The following discussion distinguishes between flexible, average, and frozen geometry models. All are reduced dimensionality models and differ in the way how the nonactive geometry parameters (i.e., those not included explicitly) are treated. In the case of the flexible models the electronic energy was minimized with respect to all inactive geometry parameters. The corresponding variation of the inactive coordinates as a function of the active ones was fully taken into account in the calculation of the covariant metric tensor. The geometry relaxation was described with a polynomial expansion in the active coordinates with expansion coefficients derived by least-squares fits. This representation is less flexible than the SASI scheme, but it guarantees smooth (analytical) higher derivatives of Cartesian coordinates. Slight wiggles in the relaxed geometries (e.g., due to the finite accuracy of the energy minimization) could otherwise produce large unphysical spikes in the pseudo-potential. Models neglecting the pseudo-potential contributions do obviously not suffer from such problems. Such models, however, may not describe the influence of geometry relaxation properly. An alternative approach would extend SASI to higher than cubic splines and combine it with a smoothing procedure. Average geometry models use the same potential as the corresponding flexible models, but replace the inactive geometry parameters by their average values when calculating $\boldsymbol{I}$, $\boldsymbol{C}$, and $\boldsymbol{g}$ (eqs 5−7). Finally, for the frozen geometry or "rigid" models the inactive geometry parameters are frozen at their average values both in the calculation of the electronic energy and in the calculation of the covariant metric tensor (eqs 5−7).

The coordinates were discretized in terms of a Chebychev−DVR[16] leading to an equidistant grid. The up to six-dimensional vibrational Schrödinger equation was solved exactly by successive diagonalization and truncation in each degree of freedom extending the scheme proposed by Bačić and Light[20] as described in more detail in refs 12 and 14. The efficiency of this method depends on the ordering of coordinates. The best choice has the fast degrees of freedom come first and the slow ones last. With an expected ground state tunneling splitting on the order of 10^{-3} to 10^{-2} cm^{-1} overall convergence is very critical here. It was checked carefully with respect to all truncation parameters by systematically increasing one cutoff limit after the other using an automated procedure. The convergence checks obviously took several times the computational effort of the single converged calculations. Table 3 lists the DVR grid parameters and the basis set truncation used in the present calculations.

Ro-vibrational eigenvalues were obtained by expanding the eigenfunctions in a direct product basis of pure vibrational (angular momentum quantum number $J = 0$) eigenfunctions $|v\rangle$ of (eq 2) with eigenvalues E_v and symmetric rigid-rotor eigenfunctions $|J\,K\rangle$. The Hamiltonian matrix elements are then given by integrating (eq 1) over $\mathbf{q}$:

$$\langle J, K'|\langle v'|H|v\rangle|J, K\rangle = \delta_{v'v}E_v + \sum_\alpha B_{\alpha\alpha}^{\ v'v}\langle J,K'|\hat{J}_\alpha^2|J,K\rangle + \sum_{\alpha<\beta} B_{\alpha\beta}^{\ v'v}\langle J, K'|\{\hat{J}_\alpha, \hat{J}_\beta\}|J, K\rangle + \sum_\alpha \zeta_\alpha^{\ v'v}\langle J, K'|\hat{J}_\alpha|J, K\rangle \qquad (9)$$

$$B_{\alpha\beta}^{\ v'v} = \frac{1}{2}\langle v'|\mu_{\alpha\beta}|v\rangle \qquad (10)$$

$$\zeta_\alpha^{v'v} = \frac{1}{2}\sum_k\langle v'|\{\hat{p}_k, Z_{k\alpha}\}|v\rangle \qquad (11)$$

To improve convergence the molecule-fixed coordinate system was rotated so as to minimize ro-vibrational interactions following the scheme proposed by Pickett,[21] which can be viewed as a generalization of the Eckart axis system[22] to large amplitude vibrations. Since C_{2h} symmetry is retained throughout one has $B_{xz}^{v'v} = B_{yz}^{v'v} = \zeta_x^{v'v} = \zeta_z^{v'v} = 0$. Given the heavy molecular frame of FAD nonvanishing $|B_{\alpha\beta}^{v'v}|$ are very small for $v' \neq v$ (typically $\sim 10^{-3}$ cm^{-1}). Therefore, it suffices to minimize the dominant Coriolis terms which here only requires rotation of the axis system around the y-axis, i.e., the c-axis. The corresponding rotation angle ϕ (not to be confused with the Euler angles of rotation) is a function of the vibrational coordinates. A simple linear form reduced the ro-vibrational interactions sufficiently to achieve the convergence acceleration necessary for the accurate numerical calculation of rotational excitation energies:

$$\phi/\text{deg} = 5\times 10^{-4}(x_H/\text{Å}) + 9\times 10^{-3}(\Delta r/\text{Å}) + 2\times 10^{-3}(\beta_R/\text{deg}) \qquad (12)$$

With this choice of body-fixed axis system rotational energies were found to converge to within 10^{-5} cm^{-1} with only a few

TABLE 4: Ground State Tunneling Splittings Δ_t Calculated for Different Multidimensional Models of FAD[a]

		min. energy potential				
			Δ_t		rigid model	
	coordinates	ΔZPE[b]	flexible	average	Δ_t	ΔE_{eff}[c]
1D	IRC	−1436	$<10^{-6}$			
	IRC_0[d]	0	5.1×10^{-5}	3.3×10^{-4}		
	(r_{OH})	−1436	$<10^{-4}$			
2D	(r_{OH}, R)	+142	$<10^{-4}$	0.1743		
	(x, R)		$<10^{-4}$	0.1318		
3D	(x, β_R, R)			0.0222		
	(x, z, R)	+52	$<10^{-4}$	0.1062		
	(x, Δr, R)				1.5162	2380
4D	(x, Δr, β_R, R)	+38	0.0001	0.0088	0.0003	3460
5D	(x, z, Δr,β_R,R)				0.0013	2940
6D	(x, z, Δr, β, β_R, R)				0.0015	2940

[a] All values are given in cm^{-1}. [b] Harmonic ZPE correction due to inactive coordinates not included in the calculation. [c] Potential energy difference between minimum and saddle point for rigid models. For all flexible models the potential barrier is 2930 cm^{-1}. [d] ZPE included in an approximate fashion as explained in the text, yielding an effective barrier height of 1494 cm^{-1}.

hundred vibrational levels included. The exact energies do of course not depend on the choice of axis system.

3. Results and Discussion

Table 4 lists the ground state tunneling splittings calculated for the different reduced-dimensionality models investigated here. The following discussion of how realistic such models can be focuses on three key questions: Which are and how to identify the degrees of freedom to include explicitly as "active coordinates"? What is the effect of geometry relaxation in the remaining degrees of freedom? What is the effect of zero point energy in the corresponding vibrational modes?

3.1. Models Including Geometry Relaxation. By construction all flexible models comprise the minimum energy tunneling path. Consequently they all feature the same barrier of 2940 cm^{-1}. As a consequence of the partial energy minimization those coordinates not included explicitly in the model ("inactive" coordinates) change as a function of the active coordinates $\{q_k\}$ (eqs 5−7). Neglecting this dependence in the kinetic energy and assuming fixed average values for the inactive coordinates in calculating G_{kl} and u' (eq 2) produces relatively large tunneling splittings. For a barrier height of more than 30 kJ/mol the proton exchange tunneling might at first glance appear surprisingly efficient, but inspecting the dynamical "zero point energy" (ZPE) contributions affords an immediate explanation. In the harmonic limit this is simply a change in the effective barrier given by half the difference between harmonic wavenumbers at the transition state and at the equilibrium, summed over all inactive degrees of freedom. Zero point effects due to the active degrees of freedom are obviously already included exactly in the ro-vibrational calculation. The harmonic wavenumbers given in Table 2 (B3LYP/6-31+G*) yield a zero point correction due to inactive coordinates (ΔZPE) of −1440 cm^{-1} almost halving the barrier height in 1D. This is the result of the "loss" of the gerade OH stretching mode accompanied by the pronounced softening of the corresponding ungerade mode. The resulting ZPE correction of about −2600 cm^{-1} is only partly compensated by the increased overall rigidity of the complex in its transition state. Closer inspection shows that the contributions of B_u (−731 cm^{-1}), B_g (+189 cm^{-1}), and A_u(+196 cm^{-1}) vibrations almost cancel, justifying the restriction of the present investigation to C_{2h} in-plane dynamics, i.e., A_g modes. Since the present calculations (except IRC_0, see below) neglect all ZPE corrections due to inactive coordinates, the tunneling splitting is negligible in the 1D calculations. The ZPE corrections may be included approximately in the IRC model by interpolating ΔZPE linearly between the minimum and the transition state, and adding it to the electronic potential. This model (IRC_0 in Table 4) yields a tiny tunneling splitting of 5.1×10^{-5} cm^{-1} for the resulting effective barrier height of about 1500 cm^{-1}. All higher dimensional models include the hydrogen transfer coordinate explicitly, so that the remaining ΔZPE becomes much smaller and, in fact, almost negligible.

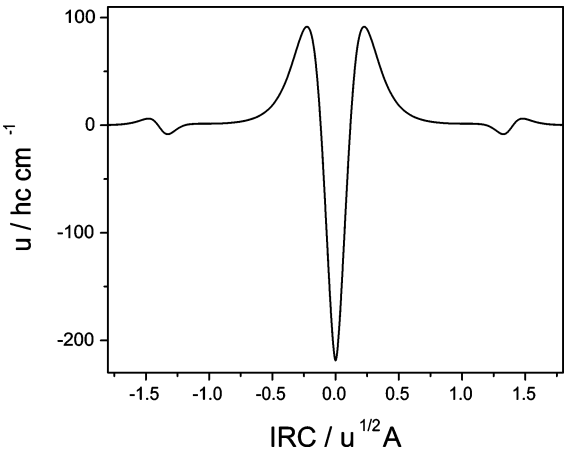

Figure 3. Pseudo-potential along the intrinsic reaction coordinate of the concerted hydrogen exchange in formic acid dimer.

Taking the geometry relaxation of the inactive coordinates explicitly into account in the kinetic energy operator (eq 2) essentially quenches the tunneling process ("flexible" models in Table 4). Within the numerical accuracy the lower dimensional models (up to 3D) yield vanishing tunneling splittings. The results clearly demonstrate the major effect the geometry relaxation has through the kinetic energy. The origin is 2-fold: (1) The effective reduced mass $\boldsymbol{g}$ (eq 7) is increased by heavy atom rearrangement. (2) The change of the frame's geometry induces large pseudo-potential terms (eq 3) through the third derivative of the Cartesian geometry wrt the active coordinates. To assess the relative importance of the two contributions I have performed calculations for the ZPE corrected IRC_0 model (see Table 4). Figure 3 shows the pseudo-potential for the 1D flexible model. Neglecting the pseudo-potential leads to an increase of the tunneling splitting by 30% to 6.7×10^{-5} cm^{-1}. The path itself is basically a consecutive motion along R and x_H. Neglecting the relaxation of all other geometry parameters in the calculation of the effective reduced mass, i.e., g in (eq 7), leads to the corresponding "average geometry model" (Table 4) with a tunneling splitting of 3.3×10^{-4} cm^{-1}. The 6-fold increase compared with the exact flexible model results from the decrease of the effective mass by about one-third. Thus, the reduced mass effect clearly dominates, but the pseudo-potential still affects the tunneling splitting very significantly. It should also be noted that the power series expansion of the inactive geometry parameters tends to smooth any high curvature sections of the path, where the geometry changes abruptly. This in turn tends to reduce the absolute value of the pseudo-potential. Once R and x_H are treated explicitly the largest curvature contributions are removed, so that the pseudo-potential is reduced drastically for all two- and higher-dimensional models. With typical values of 10 cm^{-1} in the vicinity of the reaction valley its influence on the tunneling dynamics becomes negligible. The tunneling splitting calculated for flexible models in 2D and 3D still remains negigible ($< 10^{-4}$ cm^{-1}, see Table 4)

due to the large reduced-mass effect, which is mainly due to the C=O/C−O bond length relaxation and to a lesser extent to the intermolecular bending. Once all major heavy atom relaxation modes are included (Δr and β_R) finite tunneling splittings persist. The 4D model coupling x, Δr, β_R, and R apparently captures the most important contributions to the hydrogen exchange tunneling dynamics in FAD, producing a still tiny but definitely nonvanishing tunneling splitting of 0.0001 cm^{-1}. This model includes the major heavy atom motion as well as the strong curvature in (x_H, R). Remaining ZPE corrections cancel almost completely. This cancellation should not be considered fortuitous. Rather it is a consequence of the highly local character of the hydrogen stretching motion, so that there is no significant kinetic energy coupling to the molecular frame. In addition the transformation from valence (r_{OH}, β_{OH}) to Cartesian coordinates (x_H, z_H) removes the intrinsic OH stretch/bend coupling in the kinetic energy.

There is another important conclusion to be drawn from the results obtained with the flexible models. Both the effective mass and the pseudo-potential effect are already included in the 1D model. It suffers from the neglect of large ZPE corrections, but these become small or even negligible for higher dimensional models. Still there is virtually no tunneling calculated for 2D and 3D ($< 10^{-4}$ cm^{-1}, see Table 4). The most important part of the geometry relaxation apparently has to be contained within the space of active coordinates treated explicitly to obtain an at least qualitatively correct description of the dynamics. This does not necessarily mean that the hydrogen exchange tunneling in FAD is an inherently four- or even higher-dimensional process. Rather it hints at significant "corner cutting" in degrees of freedom with large effective reduced mass which induce nonadiabatic coupling terms along the minimum energy path (see ref 23 for an instructive example). This means that in regions where the minimum energy path is strongly curved the tunneling occurs preferably at the innermost side of the curve, thus reducing curvature at the expense of higher potential energy, with the balance reducing the action along the path. This effect has long been recognized as quite ubiquitous in light atom tunneling. It might still be possible that an optimally adiabatic path minimizing the above-mentioned couplings, might provide a realistic effectively one-dimensional description of the tunneling process. Although an interesting proposition in principle, it is not obvious how to construct such a path a priori (see ref 24 for a more extensive discussion).

3.2. Rigid Models. The above conclusions were tested against calculations for rigid models constructed from the same set of degrees of freedom. By construction such rigid models are not subject to the effective mass and pseudo-potential effects discussed in the previous section. In particular the latter, which derive from higher derivatives of the geometry, are prone to artifacts that might result from slight numerical inaccuracies of the optimization procedure. Furthermore, the construction of potential energy functions is computationally much less demanding for rigid models than for flexible ones. This makes it possible to extend the calculations to higher dimensions.

Apart from the hydrogen transfer coordinate x_H (gerade OH stretch) and the monomer separation R (intermolecular stretch) significant geometrical changes along the tunneling path are limited to the in-plane hydrogen bend (z_H), the intermolecular in-plane bend β_R, and the antisymmetric OCO stretching coordinate (Δr). The change in r is by far the largest as it reflects the interchange of CO single and double bonds in the course of the hydrogen exchange. The smallest rigid model therefore includes Δr in addition to the hydrogen transfer coordinate x_H and the monomer separation R. Keeping z_H, r, and β close to their equilibrium values and β_R at zero (for the sake of symmetry) the calculation yields an enormous tunneling splitting of 1.52 cm^{-1}. It is mostly the result of enforcing C_{2h} symmetry for the molecular frame by setting $\beta_R = 0$, which shifts the minima to much higher potential energies. This is only partly offset by fixing the symmetric coordinates at the equilibrium values, so that the effective barrier height decreases by about 500 cm^{-1}. It now becomes comparable, e.g. to that of ammonia (NH_3) and so does the tunneling splitting. Including the intermolecular in-plane bend β_R in the calculations brings the minima back to (almost) zero, but with z_H still frozen at its equilibrium value, the effective barrier is now 500 cm^{-1} too high. Still a finite tunneling splitting of 0.3×10^{-3} cm^{-1} is found. This is close to the value obtained with the flexible model including the same set of active coordinates. The latter, however, features the much lower correct barrier height by construction underlining the importance of effective mass and pseudo-potential effects due to the remaining geometry relaxation. Since z_H is the only remaining coordinate that changes significantly along the tunneling path, its inclusion within a 5D model should afford a correct representation of the in-plane tunneling dynamics. The resulting tunneling splitting of 1.3×10^{-3} cm^{-1} compares reasonably well with the lower of the two experimental values for $(DCOOH)_2$ of 2.9×10^{-3} cm^{-1},[5] in particular considering that the true barrier height is presumably slightly (100−200 cm^{-1} or half a percent) lower than for the B3LYP/6-31+G* potential used in the present study. Part of this effect should even be compensated by slightly smaller ZPE corrections as anharmonicities were neglected in the above discussion. Further inclusion of the OCO bending coordinate β in a six-dimensional model leads to only minor changes compared with the results obtained in 5D.

3.3. Rotational Structure and Inertial Defects. For rigid planar structures only two of the three moments of inertia are independent as the so-called inertia defect

$$\Delta_I = I_C - I_B - I_A \tag{13}$$

must vanish, while it takes on negative values for nonplanar structures. For nonrigid molecules these conditions are relaxed even in the vibrational ground state. In the simplest picture a nonrigid molecule becomes nonplanar on average (in terms of root-mean-square deviations from planarity) due to out-of-plane zero-point vibrational motion. At best this can only be an approximate argument since even triatomic molecules feature nonvanishing Δ_I, even though there are evidently no out-of-plane modes. Still semirigid planar molecules show only small and generally negative Δ_I.

The analysis of the rotational structure of the IR diode laser spectra observed by Madeja and Havenith in a seeded free supersonic jet expansion[5] led to rotational constants corresponding to small but apparently significant negative inertia defects for the totally symmetric tunneling levels (−0.38 u Å^2 for the ground state and −0.57 u Å^2 for ν_{C-O}). The antisymmetric levels by contrast, showed systematically higher values (+0.16 and −0.02 u Å^2, respectively).[5] On the basis of this finding, the authors speculated about possible out-of-plane motion of the proton in the course of the tunneling process. Such an effect would be very surprising as ab initio quantum chemical calculations without exception yield a planar transition structure for the concerted hydrogen exchange. The saddle point structure is even more rigid with respect to out-of-plane degrees of freedom than the equilibrium structure (see Table 1). As already pointed out, simply invoking vibrational averaging over non-

TABLE 5: Single Mode Contributions to the Inertia Defect Calculated for the Vibrational Ground State of FAD from the B3LYP/6-31+G* Harmonic Force Field

in−plane					out−of−Plane				
mode[a]	$\tilde{\omega}_g$[b]	$\delta\Delta_I$[c]	$\tilde{\omega}_u$[b]	$\delta\Delta_I$[c]	mode[a]	$\tilde{\omega}_g$[b]	$\delta\Delta_I$[c]	$\tilde{\omega}_u$[b]	$\delta\Delta_I$[c]
β_R	170	0.000	269	−0.847	τ_R			78	+1.304
ν_R	210	+0.166			δ_R	257	+0.292	180	+0.561
β_{OCO}	678	+0.022	704	−0.535	δ_{OH}	956	+0.094	982	+0.089
ν_{C-O}	1254	−0.000	1255	−0.275	δ_{CH}	1069	+0.087	1090	+0.087
β_{CH}	1405	−0.093	1397	−0.133					
β_{OH}	1461	−0.129	1441	−0.323					
$\nu_{C=O}$	1723	−0.050	1786	−0.183					
ν_{CH}	3118	−0.045	3113	−0.079					
ν_{OH}	3156	−0.015	3247	−0.026					
Σ		−0.143		−2.401		Σ	+0.473	+2.041	

[a] Mode assignment; see Table 2. [b] Harmonic wavenumbers in cm^{-1}. [c] Single mode contributions to Δ_I in u $Å^2$.

TABLE 6: Rotational Constants and Inertia Defects for the Vibrational Ground State of FAD

	4D[a]		5D[a]		expt[b]	
$\tilde{\nu}/cm^{-1}$	0.0000	0.0003	0.0000	0.0013	0.0000	0.0029
A/cm^{-1}	0.201763	0.201763	0.201573	0.201574	0.20205	0.202 05
B/cm^{-1}	0.074910	0.074910	0.075024	0.075024	0.070 59	0.070 63
C/cm^{-1}	0.055706	0.055599	0.055791	0.055707	0.05237	0.05231
Δ_I/u $Å^2$	−5.97	−5.39	−6.17	−5.71	−0.38	+0.16

[a] Rigid models. Rotational constants for $(HCOOH)_2$. [b] Experimental values derived from the rotational analysis of ν_{C-O} of $(DCOOH)_2$.[5]

planar geometries cannot provide a wholly satisfactory explanation for nonvanishing Δ_I values of planar molecules (i.e., molecules with planar equilibrium structures). A more appropriate explanation was already given by Oka and Morino[25] using perturbation theory to describe vibrational effects on the rotational structure. Within the harmonic approximation the contributions of individual modes to the inertia defect in the vibrational ground state are additive (see also ref 26 (eq 24.4.3)). For the B3LYP/6-31+G* potential surface, the values are given in Table 5 adding up to an overall inertia defect of −0.0292 u $Å^2$ (within the harmonic approximation). This is significantly smaller (in absolute value) than the experimental value of −0.38 u $Å^2$ assigned to the ground state in ref 5. But as Table 5 clearly shows single mode contributions are up to 40 times larger. Moreover in-plane and out-of-plane contributions are comparable in magnitude, the latter even being positive. (For the strictly planar transition structure, i.e., excluding the transition mode, the inertia defect takes a negative value of −0.30 u $Å^2$. The physical relevance of such a quantity may, however, be debatable.) In view of this result the experimental values found by Madeja and Havenith must be considered as fairly small in magnitude and certainly compatible with an in-plane hydrogen exchange process. Going beyond the harmonic approximation is not expected to change the situation qualitatively. On the contrary, highly anharmonic large amplitude motions (LAM) are more likely to produce even larger inertia defects simply because they deviate even more from the idealized rigid behavior. Table 6 lists the rotational constants derived from four and five-dimensional models including the most important LAM degrees of freedom involved in the hydrogen exchange process. The rotational constants were deduced directly from the $J = 1$ rotational levels obtained from fully coupled ro-vibrational variational calculations as outlined in section 2. The results confirm the expectation of increased contributions to the inertia defects from LAM subspaces. They also show that these can differ markedly for the two tunneling components—here by about 0.5 u $Å^2$ for both models. The calculated values are obviously not expected to agree particularly well with the experimental values although interestingly enough the difference between the inertia defects of the two tunneling components does have the correct sign and approximately even the correct value. That might still be fortuitous. First of all the B3LYP/6-31+G* equilibrium geometry deviates slightly from the correct r_e structure. Second contributions are missing from all the remaining vibrational degrees of freedom some of which have significant Coriolis interactions with the active subspace.

4. Conclusions

The results presented in this contribution for FAD as a prototype system clearly demonstrate the importance of a proper dynamical description of the structural relaxation in hydrogen exchange tunneling processes. Neglecting the dynamical effect of geometry relaxation leads to a completely unrealistic representation of the tunneling process overestimating even ground state tunneling splittings by orders of magnitude. The structural relaxation affects the tunneling dynamics mainly through the effective mass, but the pseudo-potential still has a substantial effect on the tunneling splitting (∼30%) in 1D models, due to the substantial curvature of the path. Once the H-transfer coordinate and the inter-monomer distance are included explicitly the pseudo-potential becomes negligible, while the effective reduced mass effect persists. As a result low-dimensional adiabatic models of the tunneling process lead to practically vanishing tunneling probability. Only if all the major heavy atom motion is included explicitly realistic values are obtained for the tunneling splitting. In FAD this includes a minimum of four degrees of freedom leading to the conclusion that beyond the obvious (large-curvature) corner-cutting in the (x_H, R) plane significant corner-cutting also occurs in the antisymmetric OCO stretch and to a lesser extent in the in-plane intermolecular bend. For FAD no major adiabatic (ZPE) corrections occur due to accidental near perfect cancellation of out-of-plane and ungerade in-plane contributions. Thus, the concerted hydrogen exchange tunneling in FAD appears to be an example of near perfect in-plane dynamics. From the analysis of ro-vibrational coupling contributions it is also clear that this picture is perfectly compatible with all experimental data known so far. What remains is the question about the assignment of the tunneling components. The experiment is necessarily

ambiguous in this respect until the rotational analysis succeeds for a second transition from the vibrational ground state. Madeja and Havenith assumed the tunneling splitting to increase upon excitation of the $\nu_{C-O}(u)$ fundamental. This assignment has recently been questioned on the basis of semiclassical model calculations.[8] While the quantitative reliability of such calculations may be uncertain, their results are also supported by a qualitative argument put forward in ref 8: the exchange tunneling requires the transfer of excitation from one C−O group to another as C−O and C═O change places. This should inhibit the tunneling process compared with the vibrational ground state by analogy to similar situations such as the one discussed in ref 23. While the argument is certainly valid in principle, it relies on a local mode picture of the CO stretching vibrations, which is very much of an idealization in the case of FAD. The results obtained in the present study rather appear to support the assignment of Madeja and Havenith. The ground state tunneling splitting is calculated in 5D as 0.0013 cm^{-1}. This result is based on the B3LYP/6-31+G* barrier height of 2930 cm^{-1}. This value is presumable too high by 1−2 kJ/mol or about 5%. This would explain the factor of 2 compared with the lower of the experimental values of 0.029 cm^{-1}, but it is hardly compatible with the alterative assignment giving a 10 times larger experimental value. A more clear-cut conclusion would require calculations explicitly including the ungerade CO stretching modes in a 7D model of the hydrogen exchange tunneling in FAD.

Acknowledgment. This work has been supported financially by the Deutsche Foschungsgemeinschaft through the Sonderforschungsbereich 357. The generous allocation of CPU time at ETH Zürich and on the Western Canada Research Grid is gratefully acknowledged.

References and Notes

(1) Chamma, D.; Henri-Rousseau, O. *Chem. Phys.*. **1999**, *248*, 53.
(2) Florio, G. M.; Sibert, E. L., III; Zwier, T. S. *Faraday Discuss*. **2001**, *118*, 315.
(3) Emmeluth, C.; Suhm, M. A.; Luckhaus, D. *J. Chem. Phys.* **2003**, *118*, 2242.
(4) Florio, G. M.; Zwier, T. S.; Myshakin, E. M.; Jordan, K. D.; Sibert, E. L., III. *J. Chem. Phys.* **2003**, *118*, 1735.
(5) Madeja, F.; Havenith, M. *J. Chem. Phys.*. **2002**, *117*, 7162.
(6) Shida, N.; Barbara, P. F.; Almlöf, J. *J. Chem. Phys.* **1991**, *94*, 3633.
(7) Tautermann, C. S.; Voegele, A. F.; Liedl, K. R. *J. Chem. Phys.* **2004**, *120*, 631.
(8) Smedarchina, Z.; Fernandez-Ramos, A.; Siebrand, W. *J. Chem. Phys.*. **2005**, *122*, 4309.
(9) Coutinho-Neto, M. D.; Viel, A.; Manthe, U. *J. Chem. Phys.* **2004**, *121*, 9207.
(10) Jursic, B. S. *J. Mol. Struct. (THEOCHEM)* **1997**, *417*, 89.
(11) Tautermann, C. S.; Loferer, M. J.; Voegele, A. F.; Liedl, K. R. *J. Chem. Phys.* **2004**, *120*, 11650.
(12) Luckhaus, D. *J. Chem. Phys.* **2003**, *118*, 8797.
(13) Qian, W.; Krimm, S. *J. Phys. Chem. A* **1998**, *102*, 659.
(14) Luckhaus, D. *J. Chem. Phys.* **2000**, *113*, 1329.
(15) Harris, D. O.; Engerholm, G. G.; Gwinn, W. D. *J. Chem. Phys.*. **1965**, *43*, 1515.
(16) Dickinson, A. S.; Certain, P. R. *J. Chem. Phys.*. **1968**, *49*, 4209.
(17) Meyer, R.; Günthard, H. H. *J. Chem. Phys.* **1968**, *49*, 1510.
(18) Meyer, R.; Günthard, H. H. *J. Chem. Phys.* **1969**, *50*, 353.
(19) Lauvergnat, D.; Nauts, A. *J. Chem. Phys.* **2002**, *116*, 8560.
(20) Baciæ, Z.; Light, J. C. *Annu. Rev. Phys. Chem.* **1989**, *40*, 469.
(21) Pickett, H. M. *J. Chem. Phys.* **1972**, *54*, 1715.
(22) Eckart, C. *Phys. Rev.* **1935**, *47*, 552.
(23) Sibert, E. L., III. *J. Phys. Chem.* **1989**, *93*, 5022.
(24) Shida, N.; Almlöf, J.; Barbara, P. F. *J. Phys. Chem.* **1991**, *95*, 10457.
(25) Oka, T.; Morino, Y. *J. Mol. Spectrosc.* **1961**, *6*, 472.
(26) Papousek, D.; Aliev, M. R. *Molecular Vibrational−Rotational Spectra*, *Studies in Physical and Theoretical Chemistry*; Elsevier Scientific Publishing Company: Amsterdam, 1982.
(27) Neuheuser, T.; Hess, B. A.; Reutel, C.; Weber, E. *J. Phys. Chem.* **1994**, *98*, 6459.
(28) Landoldt-Börnstein. *Structure Data of Free Polyatomic Molecules. New Series*; Springer: Berlin, 1976; Vol. II/7.
(29) Matylitsky, V. V.; Riehn, C.; Gelin, M. F.; Brutschy, B. *J. Chem. Phys.* **2003**, *119*, 10553.
(30) Almenningen, A.; Bastiansen, O.; Motzfeld, T. *Acta Chem. Scand.* **1969**, *23*, 2848.
(31) Almenningen, A.; Bastiansen, O.; Motzfeld, T. *Acta Chem. Scand.* **1970**, *24*, 747.
(32) Harmony, M. D.; Laurie, V. W.; Kuczkowski, R. L.; Schwendemann, R. H.; Ramsay, D. A.; Lovas, F. J.; Lafferty, W. J.; Maki, A. G. *J. Phys. Chem. Ref. Data* **1979**, *8*, 619.